Article ID:1007－6492(2000)02－0001－08

Effects of Solidification Kinetics on the Phase Composition in Ni－Al System

SHEN Ning－fu, LIANG Chang－hao, LI Jian－qiang, WANG Xi－ke, SHI Guang－xin

(Research Center for Materials, Zhengzhou University of Technology, Zhengzhou 450002, China)

Abstract: Rapidly solidified ribbons of Al－20～80 at. % Ni alloys were obtained by planar flow casting. The phase composition and microstructure of the melt－quenched ribbonswere investigated by X－ray diffraction and transmission electron microscopy. The fractions of occurring phases in the rapidly solidified ribbons differed significantly from that in the conventional cast ingots. In the Al－rich alloys, the fraction of the α－Al solid solution decreased drastically due to rapid solidification. Among all the intermediate phases, the fractions of intermediate phases with lower liquidus temperature increased (Al_3Ni in relation to Al_3Ni_2, Al_3Ni_2 in relation to AlNi). All observed intermetallic compounds Al_3Ni, Al_3Ni_2 and AlNi in the as－quenched samples contained less Ni content in comparison with the equilibrium data and conventional castings. In the Ni－rich alloys, the fraction of $AlNi_3$ increased and the fraction of AlNi decreased. The effects of melt－quenching on the phase composition were explained on the basis of kinetic analyses of nucleation and dendrite growth of various intermetallic compound phases. The nonequilibrium solute partitioning and solute trapping during rapid continuous cooling lead to the increase of the effective alloy concentration for the phases with lower equilibrium liquidus temperature, which favored both the nucleation and growth of these secondly solidified phases.

Key words: Al－Ni alloy; rapid solidification; phase composition

CLC number: TQ 032.41 **Document code**: A

Introduction

The current interest in intermetallic compounds centers on their potential as new high－temperature structural materials with high melting temperature, comparatively low density, good oxidation resistance and extreme hardness . A major drawback of these materials is their room－temperature brittleness, which may be alleviated by controlling of the phase composition and microstructure directly affected by the kinetic process of solidification. Cahn et al. have shown that a noneqilibrium degree of long－range chemical order or a fine pattern of anti－phase domains might improve the ductility. One route to noneqilibrium structure is rapid solidification. Boettinger and Aziz[1] have shown that the extension of solute trapping theory to the sublattices in an ordered compound leads to a prediction of disorder trapping at high solidification velocities. As the solidification velocity is increased, the loss of interface equilibrium leads not only to solute trapping, but also to a reduction of the degree of long－range chemical order. In the last few years a series of theoretical and experimental works[2～5] have been reported for the Ni－Al system in the composition range around AlNi and $AlNi_3$ to investigate the effects of the deep undercooling on the structure features of intermetallic compounds. Recently, Assadi et al[6] presented an analysis of the solidification kinetics of the $L1_2$ and B2 phases in the Ni－rich part of the Ni－Al system. In their paper, based on disorder－trapping and dendrite－growth models, the growth velocity, the composition at the solid/liquid interface and the long－range order have been calculated as a function of alloy composition and undercooling, and experimental studies on the competitive phase selection and growth behavior of these intermetallic compounds and disordered f. c. c. solute solution have been per-

Received date: 1999－10－10; **revision received date**: 2000－01－11

Foundation item: Supported by the Natural Science Foundation of China(59771033)

Biography: SHEN Ning－fu(1935－), male, born in Shanghai, professor of Zhengzhou University of Technology, doctorate instructor, research interests: metastable materials.

formed using the electromagnetic levitation deep undercooling technique.

Along with the high－temperature structural applications, the intermetallic compounds are also used for various structural and functional applications. For example, Al－rich alloys are used as precursor alloys for skeleton catalysts, in which the phase composition and microstructure features of the precursor alloys affected by the kinetic process of solidification play an important role in the control of the catalytic properties of prepared catalysts. These precursor Al－Ni alloys usually involve the composition range around Al－25～35 at. % Ni, leading to the appearance of Al_3Ni, Al_3Ni_2, AlNi, α－Al and other metastable Al－rich intermetallic phases. Comparatively only limited works[7,8] have been reported on the solidification kinetics and phase selection in the Al－rich part of the Ni－Al system.

Most of the published works in the Al－Ni system focused on a single solidification step at certain undercooling using the electromagnetic levitation deep undercooling technique, with which direct kinetic measurements could be performed quantitatively. Although the results can be applied to elucidating the primary phase selection at certain undercooling, the prediction of the entire phase composition as the result of continuous cooling melt－quenching still remains for further investigation. Besides, the melt－quenching is the main feasible industrial means to produce rapidly solidified alloys in large quantity at the present period and for the years coming on. The present paper presents experimental investigations of melt－quenched Al－Ni alloys with 20 to 80 at. % Ni, intending to elucidate the effects of solidification kinetics on the entire phase composition and microstructure features in both Al－rich and Ni－rich alloys within current theories of nonequilibrium solidification of intermetallic compounds, considering all possible steps of nucleation/growth competition between different phases during continuous cooling of melt－quenching.

1 Experimental Methods

Preliminary alloys of Al－x at. %Ni with $x=20$, 23.5, 27.5, 31.5, 36, 70, 75, 80 were prepared from pure elements Al and Ni by vacuum induction melting under argon atmosphere (40 kPa). The prepared liquid Al－Ni alloys of different chemical composition were cast into conventional metal molds with the ingot diameter of 12 mm. The estimated average cooling rate was about 10 K/sec. From these ingots rapidly solidified samples were produced by the planar flow casting technique. Thus obtained alloy ribbons were 50－70 μm in thickness and 3～5 mm in width, for which the estimated average cooling rate was about 6×10^5 K/sec. The phase composition of the ingot and ribbon samples of different chemical composition were investigated by X－ray diffraction (XRD) measurements with a Philips PW1700 diffractometer, using Cu－Kα radiation. Both massive and powdered specimens were used for investigation. The microstructures of ribbon and ingot samples were investigated by optical metallography and transmission electron microscopy with a JEM 2000－FX analytical electron microscope equipped with an EDXS system. The TEM thin foil specimens were prepared by ion beam thinning.

2 Experimental Results

Fractions of the occurring phases in conventional cast ingots and rapidly solidified ribbons of the investigated alloys as measured by X－ray diffraction are summarized in Tab. 1 and Tab. 3. In Tab. 1 the complete equilibrium phase fractions for each alloy calculated in accordance with the existing Al－Ni equilibrium phase diagram are also listed in comparison with the experimental nonequilibrium results. In Tab. 3 the phase fractions measured in annealed samples are listed.

2.1 Al－rich alloys

In Tab. 1 considerable differences in phase occurrence induced by the kinetic factors of solidification processing can readily be seen. Obviously, the phase composition in the conventional ingots is far from that in the equilibrium state. In comparison with conventional ingot casting, rapid solidification processing tends to alter the fractions of occurring phases mainly in two aspects: reducing α－Al solid solution and increasing the relative portion of intermediate intermetallic compounds with lower liquidus temperature (Al_3Ni in relation to Al_3Ni_2, Al_3Ni_2 in relation to AlNi), which is most prominent in alloys $Al_{80}Ni_{20}$, $Al_{76.5}Ni_{23.5}$ and $Al_{72.5}Ni_{27.5}$. All the observed intermediate phases in X－ray diffraction measurements were identified as ordered intermetallic compounds, although lowering of the degree of long－range order was observed,

especially for the phase Al_3Ni_2. Besides, a monoclinic metastable phase (close to Al_9Ni_2 as reported by Pohla[7]) has been observed in rapidly solidified $Al_{80}Ni_{20}$ ribbons, and a quasicrystalline decagonal phase was observed in rapidly solidified $Al_{80}Ni_{20}$, $Al_{76.5}Ni_{23.5}$ and $Al_{72.5}Ni_{27.5}$ alloy ribbons. The structural similarities have been identified between the Al_3Ni_2 ($D5_{13}$) and the metastable decagonal phases, and also between the Al_3Ni (DO_{20}) and the metastable Al_9Ni_2 phases. In Tab. 1 both metastable phases have been included into the structurally related stable phases.

Table 1 XRD measured fractions (wt.%) of occurring phases in cast ingots and rapidly solidified ribbons of Al-rich alloys

Alloy		α-Al	Al_3Ni	Al_3Ni_2	AlNi
$Al_{80}Ni_{20}$	ribbon	13.8	32.0	54.2*	
	ingot	32.7	19.1	48.2	
	equil.	16.7	83.3		
$Al_{76.5}Ni_{23.5}$	ribbon	3.4	69.1	27.5*	
	ingot	19.9	26.4	53.7	
	equil.	4.8	95.2		
$Al_{72.5}Ni_{27.5}$	ribbon		28.9	59.7*	11.4
	ingot	11.1	18.3	54.5	16.1
	equil.		76.9	23.1	
$Al_{68.5}Ni_{31.5}$	ribbon		13.3	84.1	2.6
	ingot	3.2	10.2	82.1	4.5
	equil.		38.5	61.5	
$Al_{64}Ni_{36}$	ribbon		2.4	93.9	3.7
	ingot		3.8	91.1	5.1
	equil.			100	

* Decagonal phase included.

TEM micrographs and SAED patterns of rapidly solidified samples $Al_{76.5}Ni_{23.5}$ and $Al_{72.5}Ni_{27.5}$ show that in the rapidly solidified $Al_{76.5}Ni_{23.5}$ alloy the primary grains of Al_3Ni_2 and the Al_3Ni grains were in the size range of 200~400nm, while smaller particles of Al_3Ni (40~50 nm) mixed with α-Al appeared in the intergranule regions. In the rapidly solidified $Al_{72.5}Ni_{27.5}$ alloy the microstructure varied among different microareas. The primary AlNi (only in small portion) and Al_3Ni_2 grainsformed as matrix, while a part of Al_3Ni grains seemed to be precipitated from the Al_3Ni_2 phase during subsequent cooling in the solid state, which was confirmed by a polycrystalline SAED pattern of an Al_3Ni area. EDXS measurements of the chemical composition of occurred phases gave some semiquantitative results as shown in Tab. 2, which were confirmed by the matter balance of component elements Al and Ni in the overall alloy . Rapid solidification induced the decreasing of Ni content in all three intermetallic compounds Al_3Ni, Al_3Ni_2 and AlNi. The most prominent departure from the equilibrium was observed for the Al_3Ni_2 phase in the alloys $Al_{80}Ni_{20}$, $Al_{76.5}Ni_{23.5}$ and $Al_{72.5}Ni_{27.5}$. Considering the existence of metastable Al_9Ni_2 and decagonal phases as well as the nonequilibrium extending of the chemical composition ranges of occurring phases as the result of solute trapping, these results seem to be understandable.

Table 2 Ni Contents (at.%) of phases in rapidly solidified Al-Ni alloys

Alloy	α-Al	Al_3Ni	Al_3Ni_2	AlNi
$Al_{80}Ni_{20}$	2-4	22-24	25-28*	
$Al_{76.5}Ni_{23.5}$	3-5	23-24	27-30*	
$Al_{72.5}Ni_{27.5}$		24-26	28-30*	35-37
$Al_{68.5}Ni_{31.5}$		24-26	32-34	40-42
$Al_{64}Ni_{36}$		24-26	35-37	40-42

* Mean value of "Al_3Ni_2 + decagonal phase"

2.2 Ni-rich alloys

XRD measurements (Tab. 3) show that in alloys $Al_{30}Ni_{70}$, $Al_{25}Ni_{75}$ and $Al_{20}Ni_{80}$ the occurring phases were ordered AlNi (β, B2), ordered Ni_3Al (γ′, $L1_2$) and disordered solid solution γ. The $L1_0$ martensite was the product of phase transformation of the β phase in the solid state[9].

Table 3 XRD measured fractions (wt.%) of occurring phases in Ni-rich alloys

Alloy		β ord. b.c.c., B2	β martensite f.c.t., $L1_0$	γ′ ord. f.c.c., $L1_2$	γ disord. f.c.c., A1
$Al_{30}Ni_{70}$	ribbon	28.5	26.2	45.3	
	ingot	47.8	34.4	17.8	
	anneal.	25.6		74.4	
$Al_{25}Ni_{75}$	ribbon	10.5	5.1	84.4	
	ingot	32.2	14.2	53.6	
	anneal.			100.0	
$Al_{20}Ni_{80}$	ribbon			100.0	
	ingot			100.0	
	anneal.			70.3	29.7

Again, as in the Al－rich alloys, considerable differences in phase composition induced by the kinetic factors of solidification have been observed in the Ni－rich alloys. In alloys $Al_{30}Ni_{70}$ and $Al_{25}Ni_{75}$, conventional cast ingots contained much less fraction of γ' than in annealed samples refereed to as equilirium state, correspondingly the fraction of β increased prominently. In contrast with the ingots, the melt－quenching has induced more fraction of the γ' phase. In the $Al_{20}Ni_{80}$, both the ingot and the ribbon samples were found to be consisted of single γ' phase, while the annealed sample contained disordered γ phase beside the ordered γ' phase. Although all the f. c. c. phase in melt－quenched samples has been identified as a ordered γ' phase, actually different degrees of long－range order have been determined by XRD measurements, in which the X－ray diffraction intensities I of one supperlattice {for γ' : (110)} and the corresponding fundamental peak {(220)} are determined using as a reference the ratio $I(110)/I(220) = 0.38$ in the case of complete order ($\eta = 1$) and the expression

$$\eta = \frac{4x_B^{Al} - 1}{3} = \left[\frac{I(110)}{I(220) \times 0.38}\right]^{1/2}, \quad (1)$$

Here, x_B^{Al} is the fraction of Al atoms in sublattice B of the $L1_2$ structure. The determination of η according to eqn. (1) leads to the values of η as from 0.4 to 0.99 in ingots and ribbons of different alloys (shown in Tab. 4).

Table 4 XRD measurements of degrees of long－range order (η) in γ'－$AlNi_3$ phase

Alloy		$Al_{30}Ni_{70}$	$Al_{30}Ni_{70}$	$Al_{30}Ni_{70}$
η value	ingot	0.89	0.93	0.99
η value	ribbon	0.40	0.52	0.75

The results in Tab. 4 show that the η value decreased as the solidification velocity increased and the decrease of the η value was most prominent in the $Al_{30}Ni_{70}$. There are possibly some problems with the interpretation of the XRD results since they may present an average value over regions of different composition and degrees of order. In the present case the measured values of η might be an average over regions of ordered γ' and disordered γ.

Fig. 1(a) is a TEM micrograph of an $Al_{30}Ni_{70}$ ribbon sample. SAED patterns from different grains have shown the occurrence of γ', β and β－martensite. Fig. 1(b) is the SAED pattern from a γ' grain ("A" in Fig. 1(a)). The TEM micrograph of an $Al_{25}Ni_{75}$ ribbon sample is shown in Fig. 1(c) The SAED pattern from a grain ("A" in Fig. 1(c)) is shown in Fig. 1(d) in the beam direction of [112], where supperlattice spots can be recognized.

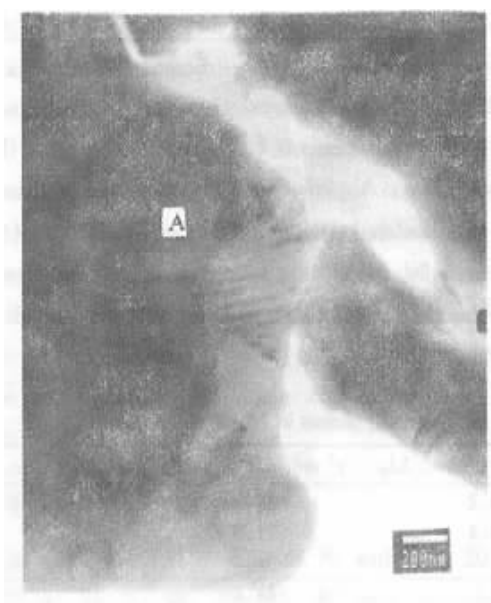

(a) TEM micrograph of $Al_{30}Ni_{70}$ ribbon, $\gamma' + \beta + \beta'$ grains

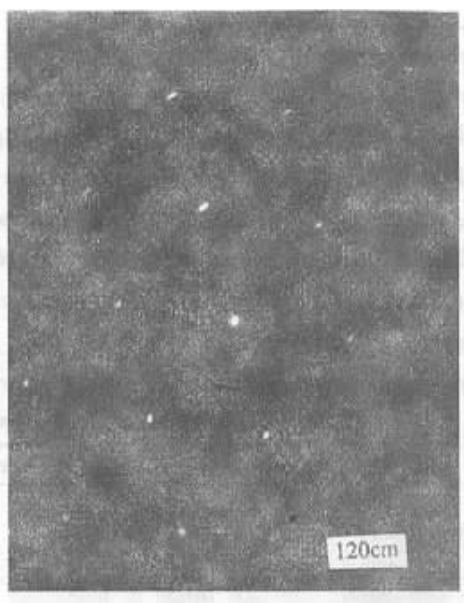

(b) SAED pattem of γ' grain A in(a), [011]

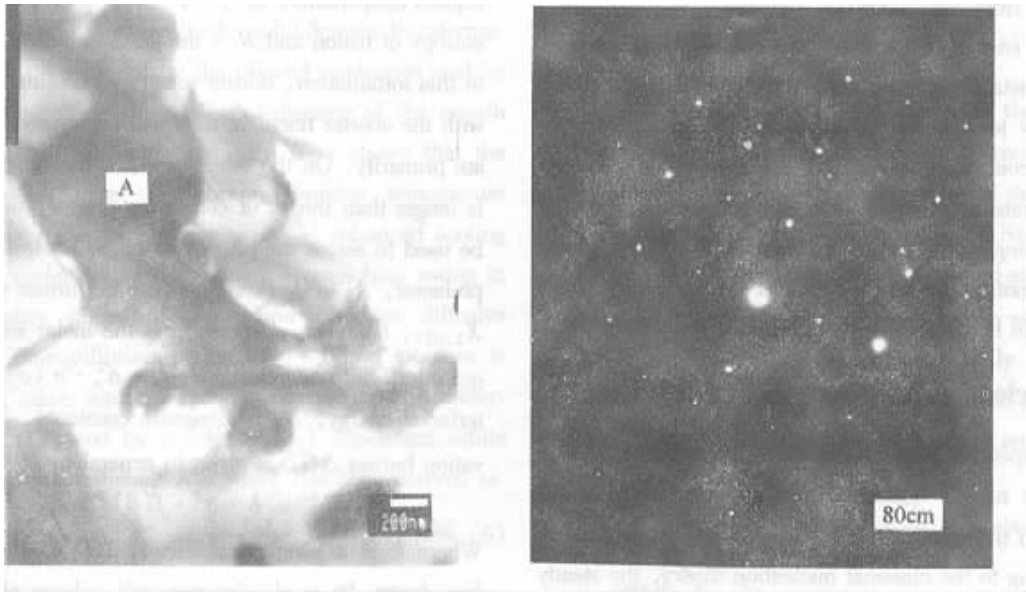

(c) TEM micrograph of $Al_{25}Ni_{75}$ ribbon, $\gamma' + \beta + \beta'$ grains

(d) SAED pattem of γ' grain A in(c), [112]

Fig. 1 TEM micrographs and SAED patterns of Ni-rich alloy ribbons

3 Solidification Sequence in Al-rich Alloys

The finally formed phase composition of Al-Ni alloys with different chemical compositions can be interpreted if all subsequently occurred processes of phase transformation are taken into consideration. In the cases of conventional cast ingots of Al-rich alloys, the lag of peritectic reactions AlNi + L → Al_3Ni_2 and Al_3Ni_2 + L → Al_3Ni has caused the remaining of the primary phases (Al_3Ni_2 in alloys $Al_{80}Ni_{20}$ and $Al_{76.5}Ni_{23.5}$, AlNi in alloys $Al_{72.5}Ni_{27.5}$, $Al_{68.5}Ni_{31.5}$ and $Al_{64}Ni_{36}$) in the final microstructures and the existence of more Al-rich melt at lower temperature than in the equilibrium process, resulting in eutectic reaction and more α-Al/Al_3Ni mixture in the microstructure, which should not happen according to the overall alloy composition and the equilibrium phase diagram. Taking the example of the alloy $Al_{80}Ni_{20}$, after 48.2 wt. % of the whole alloy (Tab. 1) solidified as primary Al_3Ni_2, the remnant melt should have reached the composition of Al-16.4 wt. % Ni calculated using the lever rule. Assuming that the further transformation of the remnant melt proceeded in a near-equilibrium way. It should have resulted in 20.2 wt. % of Al_3Ni and 31.6 wt. % of α-Al, which were very close to the XRD measured values (19.1 wt. % and 32.7 wt. % respectively, Tab. 1).

For the same alloy under rapid solidification, higher cooling rate and larger initial undercooling resulted in 54.2 wt. % of primary Al_3Ni_2 with the nonequilibrium Ni content of 25~28 at. % (Tab. 1 and 2). Using the same lever rule, the composition of the remnant melt could be calculated as Al-26.7% Ni. Taking the experimentally determined Ni content of the Al_3Ni phase as 22 at. % or 38 wt. % (Tab. 1) and assuming that the further eutectic reaction took place, the whole microstructure should have composed of 32.2 wt. % Al_3Ni and 13.6 wt. % of α-Al (with the Ni content expanded to 2 at. %, Tab. 2) beside 54.2 wt. % of Al_3Ni_2, which were also very close to the XRD measured values (32.0 wt. % and 13.8 wt. % respectively. see Tab. 1). The smaller fraction of α-Al and relatively larger fraction of the Al_3Ni phase in the ribbon can be explained by the fact that there was lower Ni content both in Al_3Ni_2 and Al_3Ni phases especially in Al_3Ni_2 owing to the nonequilibrium solute partitioning under rapid solidification condition, which caused the remnant liquid less depleted in Ni and the further reduction of the eutectic portion. Similar solidification sequence analyses can be carried out for $Al_{76.5}Ni_{23.5}$, $Al_{72.5}Ni_{27.5}$ and others. In the case of $Al_{76.5}Ni_{23.5}$ ribbon, the increasing of the Al_3Ni portion in the microstructure was even more prominent and the absolute value of the Al_3Ni_2 portion decreased in comparison with the

case of cast ingots, which can be explained by the metastable extension of the" $Al_3Ni + L$ "phase boundary to a higher temperature and by the kinetic factors controlling nucleation and growth under high cooling rate in the melt spun ribbons, resulting in the suppressing of the further growing of the Al_3Ni_2 phase and promoting the solidification of the secondary phase Al_3Ni (to be detailed in next section).

4 Nucleation and Growth Competition

The competitive formation of different crystalline phases from the rapidly quenched and undercooled melt depends on the comparative nucleation and growth rates. According to the classical nucleation theory, the steady state nucleation rate (Js) is given by the expression

$$J_S = A_S \cdot \exp(-\Delta G^*/kT), \qquad (2)$$

Where ΔG^* is the activation threshold for the formation of a critical nucleus, A_S is a prefactor, k is Boltzmann constant and A_S is temperature. Both A_S and ΔG^* can be derived for different conditions. Interpretations of the classical theory assume a constant nucleation rate, which is adequate provided the cluster populations evolve sufficiently rapidly as the temperature changes. During rapid solidification at large cooling rates this may not be always the case, and the time dependent nucleation analysis may become more reasonable. Based on works in these respects under isothermal conditions, the time (t) dependent nucleation rate J_t can be related to the steady state nucleation rate J_S. If τ is the time lag, when $t \geqslant 5\tau$, J_t reaches very closely to steady state value J_S. The transient time t_{tr} ($t_{tr} = 5\tau$) for heterogeneous nucleation in undercooled alloy melts can be given by the expression

$$t_{tr} = \frac{7.2Rf(\theta)}{1-\cos\theta} \cdot \frac{a^4}{d_a^2 \cdot X_{L,eff}} \cdot \frac{T_r}{D_L \cdot \Delta S_m \cdot \Delta T_r^2}, \qquad (3)$$

where $f(\theta)$ is a function of the contact angle θ involved in heterogeneous nucleation, $X_{L,eff}$ is the effective alloy concentration taken as either $X_{L,A}/X_{S,A}$ when nucleus is rich in A or $X_{L,B}/X_{S,B}$ when the nucleus is rich in B for a binary system, d_a is the average atomic diameter of the solid phase, a is the atomic jump distance (of the order of interatomic distance), D_L is diffusivity in the liquid, $T_r = T/T_M$, T_M is the liquids temperature, $\Delta T_r = 1 - T_r$, ΔS_m is the molar entropy of fusion and R is the gas constant. According to this formulation, during very rapid cooling, a phase with the shorter transient time will be favored to nucleate primarily. On the other hand, if the time duration is longer than the t_{tr} of competing phases, the J_S can be used to assess the priority of phase nucleation. The prefactor, A_S in J_S expression can be further related to $X_{L,eff}$., θ and σ_m, where σ_m is the molar solid - liquid interfacial energy, $\sigma_m = N_A \cdot d_a^2 \cdot \sigma$ (σ is the interfacial energy, N_A is Avogadro constant). The activation barrier ΔG^* is given in general by

$$\Delta G^* = b \cdot \sigma^3 \cdot f(\theta)/\Delta G_v^2, \qquad (4)$$

Where b is a geometrical factor, ΔG_v is the driving free energy for nucleation per unit volume of product phase. The thermodynamic driving force increases with the normalized level of undercooling ΔT_r ($\Delta T_r = (T_m - T)/T_m = \Delta T/T_m$). Furthermore, σ is related to the molar value of the latent heat ΔH_m, molar volume V and N_A by

$$\sigma = \frac{\alpha \Delta H_m}{V^{2/3} N_A^{1/3}}, \qquad (5)$$

Where α is a structure dependent factor. According to equation (3), in the transient regime, at constant θ, the decisive parameters for the preference of one phase to nucleate are the melt undercooling ΔT, as well as ΔS_m and $X_{L,eff}$. According to equation (2), (4) and (5), in the steady state regime, these decisive parameters are the melt undercooling ΔT, liquid - solid interfacial energy σ and $X_{L,eff}$. The entropy of fusion term ΔS_m plays opposite roles in the transient and/or steady state regime. While a phase of large ΔS_m will be favored to nucleate due to its shorter t_{tr}, a phase of low ΔS_m will be favored owing to the lower ΔG^*. For the investigated alloys in the present work, the competing phases Al_3Ni, Al_3Ni_2 and AlNi are all ordered intermetallic compounds. The differences in calculated values of ΔS_m for these phases are quite small. Therefore , the ΔS_m was not probably the effective decisive parameter. The structure dependent factor α in σ expression is unfortunately not exactly known at the present stage of investigation. Thus ΔT and $X_{L,eff}$ are considered to be responsible for the nucleation competition in the investigated Al - rich Ni - Al alloys whether it is in the tran-

sient or steady state regimes.

The priority of a phase in the solidification transformation can be achieved by the favored nucleation and/or the enhanced growth rate. Calculations of the growth rate for Al_3Ni, Al_3Ni_2 and AlNi have shown that the phase with lower equilibrium liquidus temperature grows with a relatively higher rate at enhanced cooling rate or undercooling during melt－quenching owing to the higher values of $X_{L,eff}$ and interface diffusive speed. Nonequilibrium at the solid－liquid interface is usually taken into consideration by the kinetic undercooling ΔT_k and by a velocity (v) dependent solute distribution coefficient K_v, which has been derived as

$$K_v = \frac{K_e + P_i}{1 + P_i}, \qquad (6)$$

Where $P_i = a_0 v / D_i$, P_i is the interface Peclet number for solute redistribution, D_i is the interface diffusion coefficient, a_0 is of the order of interatomic distance and K_e is the equilibrium solute distribution coefficient. At low velocities P_i is much smaller than 1 or K_e, so that $K_v = K_e$, whereas at very large velocities P_i is much larger than 1 or K_e, so that $K_v = 1$. Obviously, the decreasing of the Ni content in the intermediate phases in the rapidly solidified Al－rich ribbons has been caused by the higher cooling rate, larger undercooling and higher growth rate.

During the melt－quenching of the Al－rich alloy ribbons the initial undercooling could not reach the temperature lower than the metastable liquidus lines of Al_3Ni in alloys $Al_{80}Ni_{20}$ and $Al_{76.5}Ni_{23.5}$ or Al_3Ni_2 in alloys $Al_{72.5}Ni_{27.5}$, $Al_{68.5}Ni_{31.5}$ and $Al_{64}Ni_{36}$. Therefore the primary solidification of the phases Al_3Ni_2 or AlNi was not avoidable. After the first recalescence the remnant melt cooled continuously to the temperature below the metastable liquidus lines of Al_3Ni or Al_3Ni_2, when the nucleation and competitive growth of the secondary phases became possible. Although the undercooling for the primary phases was larger than for the secondary phases, but the value of $X_{L.eff}$ is much larger for the secondary phases, which favored both the nucleation and the growth of the secondary phases. The higher the cooling rate, the shorter was the time duration for the first step of solidification of single primary phase, resulting in more space for the secondary phases Al_3Ni and Al_3Ni_2.

5 Knetic Analyses of Soledifcation in Ni－rich Alloys

Fig. 2 is a calculated Ni－rich part of the Ni－Al phase diagram[6], based on the thermodynamic model of Ansara and Dupin[10] and on the model described in [6] for the b. c. c. phase. For alloys $Al_{30}Ni_{70}$ and $Al_{25}Ni_{75}$, the conventional cast ingot contained smaller portion of the γ'－$AlNi_3$ phase in comparison with the annealed sample. The difference was mainly caused by the sluggishness of the $\beta \rightarrow \gamma'$ transformation in the solid state. The occurrence of β martensite was an indication to it.

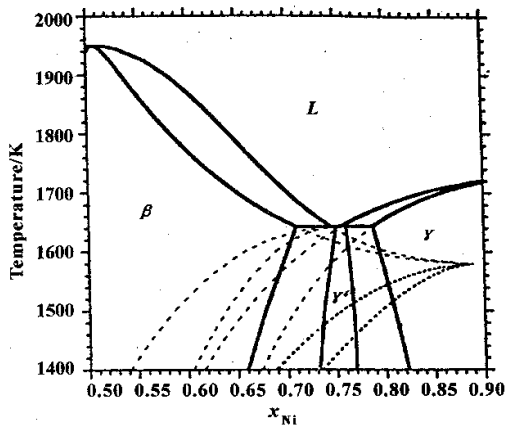

Fig. 2 Calculated Ni－rich part of the Ni－Al phase diagram

The stable equilibrium boundaries are shown as solid lines, metastable extensions of these are dashed lines, and the unstable equilibrium between the disordered b. c. c. phase and the liquid is represented by the dotted lines.

According to Fig. 2, at the composition of $Al_{30}Ni_{70}$, the metastable liquidus temperature for γ' is 60 K degrees lower than the stable liquidus temperature for β. During the melt－quenching with the cooling rate of $\sim 10^6$ K/sec, the primary nucleation of β was not avoidable. After the first recalescence the remnant melt richer in Ni cooled continuously to the temperature below the metastable liquidus temperature for γ'. At this stage of solidification, although the higher S/L interface energy for f. c. c. structure should not favor the nucleation of γ'－$AlNi_3$, but the effective alloy concentration $X_{L.eff}$ reached very closely to 1 for the γ' phase, which favored both the nucleation and growth of the γ' phase, leading to the increase of the phase fraction of γ' in the microstructure of

melt－quenched ribbons.

For the alloy $Al_{25}Ni_{75}$, the metastable liquidus temperature of the β phase is 8 K lower than the liquidus temperature of the γ′ phase. With the initial undercooling larger than 8 K, which was certainly the case during melt－quenching, the competitive nucleation and growth occurred at the first stage of solidification. Due to the similar reasons as for the alloy $Al_{30}Ni_{70}$, the phase fraction of γ′ increased with the increase of cooling rate. It is worth mentioning that this trend can not be extended to further enhanced undercooling, for instance, in the case of deep undercooling experiments.

6 Conclusions

(1) The phase composition in cast ingots (12 mm in diameter) of Al－Ni alloys is considerably different from that in equilibrium state.

(2) For both Al－rich and Ni－rich Al－Ni alloys, rapid solidification by melt－quenching leads to the increase of the fractions of intermetallic compounds with lower equilibrium liquidus temperature.

(3) The larger values of the effective alloy concentration for the phases with lower equilibrium liquidus temperature as the result of nonequilibrium solute partition and solute trapping play a major role in the changes of the phase composition in the case of melt－quenching with mild initial undercooling.

References:

[1] BETTINGER W J, AZIZ M J. Theory for the trapping of disorder and solute inintermetallic phases by rapid solidification [J]. Acta Metall, 1989, 37(12): 3379－3391.

[2] BARTH M, WEI B, HERLACH D M, et al. Rapid solidification of undercooled Ni－Al melts [J]. Materials Science and Engineering, 1994, 178: 305－307.

[3] ASSADI H, GREER A L. Application of disorder trapping to the solidification of Ni_3Al [J]. ISI J International, 1995, 35(6): 574－579.

[4] GREER A L, ASSADI H. Rapid solidification of intermetallic compounds [J]. Materials Science and Engineering, 1997, 226: 133－141.

[5] ASSADI H, GREER A L. Modelling of kinetics of solidification of intermetallic compounds [J]. Materials Science and Engineering, 1997, 226: 70－74.

[6] ASSADI H, BARTH M, GREER A L, et al. Kinetics of solidification of intermetallic compounds in the Ni－Al system [J]. Acta Mater, 1998, 46(2): 491－500.

[7] POHLA C, RYDER P L. Crystalline and quasicrystalline phases in rapidly solidified Al－Ni alloys [J]. Acta Mater, 1997, 45(5): 2155－2166.

[8] SHEN N F, TANG Y L, LIANG C H, et al. Phase structure of rapidly solidified Al－rich Ni－Al precursor alloys for catalysts [A]. IMAM MA. Advanced Materials and Processing [C]. Warrendale: TMS, 1998.

[9] LI J Q, SHEN N F, TANG Y L. Phase composition of Ni－rich Ni－Al alloys under different solidification conditions [J]. J Zhengzhou Univ Techn, 1999, 20(1): 26－28.

[10] DUPIN N. Thermodynamic model of the Ni－Al system [D]. Grenoble: Institute National Polytechnique de Grenoble, 1995.